# Stability analysis of a resonant triad in a stratified uniform shear flow

Lima Biswas [*] and Priyanka Shukla [†]
*Department of Mathematics, Indian Institute of Technology Madras, Chennai 600036, India*

(Received 16 February 2020; accepted 6 January 2021; published 25 January 2021)

The amplitude equations governing the temporal evolution of internal waves forming a resonant triad in a two-dimensional inviscid stably stratified uniform shear flow, bounded between two infinite horizontal parallel plates, are derived in the absence of diffusive effects. The density is considered to be a linear function of the vertical coordinate. The interaction of two vertically confined and horizontally propagating primary internal waves having the same frequency is considered. Specifically, for different local Richardson numbers, we show the existence and stability of the resonant triad formed by three different internal waves having the wave vector and frequency pairs as $(\vec{k}_m, \omega)$, $(\vec{k}_n, \omega)$, and $(\vec{k}_m + \vec{k}_n, 2\omega)$. For each resonant triad, we solve the amplitude equations numerically as an initial value problem. The equilibrium solutions of the amplitude equations are obtained analytically. Furthermore, the linear stability analysis of the resonant triads, around the equilibrium solutions, is carried out for various interaction cases. The triads containing a wave with the lowest mode number are found to be linearly unstable. The exact solutions of the amplitude equations are presented under the pump-wave approximation, in which the amplitude of one of the waves in the triad is larger than the amplitudes of the other two waves initially. From the exact solutions, the amplitudes of the waves forming a resonant triad are found to be unbounded when the wave with the mode number 1 acts as the pump wave. The present study helps one to have a better understanding of the stability of resonant triads of internal waves formed in a stratified shear flow.

DOI: 10.1103/PhysRevFluids.6.014802

## I. INTRODUCTION

Stratified flows are encountered everywhere in nature, for instance, in the atmosphere, oceans, and lakes. Stratified flows occurring in nature are usually stably stratified—a class of stratified flows in which the mean density increases in the direction of gravity. A disturbance in a stably stratified flow produces gravity waves driven by the restoring action of buoyancy forces and appear spontaneously at the interior parts of the flow in the form of internal waves. Internal waves in the atmosphere and ocean may develop, for instance, by blowing wind over a mountain and by tides, respectively [1–4]. Internal waves play an important role in atmospheric and oceanic circulation [5–8]. In particular, internal waves in the ocean break down to turbulence and lead to small-scale ocean mixing, which is crucial to oceanic circulation [7] that enhances marine productivity and affects the global climate [5,6,8–11].

The linear stability of stably stratified flows has been studied for decades by a number of researchers. Taylor [12] and Goldstein [13] analyzed the linear stability of inviscid shear flow in an exponentially stratified medium and derived the linearized disturbance equation, referred to as the Taylor-Goldstein equation. Taylor [12] stated that the sufficient condition for the stability of

[*] ma16d003@smail.iitm.ac.in
[†] priyanka@iitm.ac.in

 

inhomogeneous shear flow is that the local Richardson number Ri, defined as being the ratio of the buoyancy term to the flow shear term, must be higher than 0.25 everywhere in the domain. In another study, Case [14] examined the stability of an inviscid stratified shear flow in an idealized atmosphere and concluded that (i) the perturbation decays as $1/\sqrt{t}$ for Ri $> 0.25$, where $t$ denotes time, and (ii) there exists an infinite number of distinct neutrally stable eigenvalues [15]. A more general case that includes viscosity in a uniformly stratified medium was undertaken by Davey and Reid [16].

A nonlinear theory becomes important when the amplitude of the "wavelike" perturbation becomes finite [17]. Due to finite amplitude perturbations, wave interactions take place, which are responsible for the redistribution of energy among different interacting waves [18]. Wave interactions among finite-amplitude surface gravity waves on deep water were presented by Phillips [19] and furthered by Longuet-Higgins [20] and Hasselmann [21]. The focus of their studies was to understand the evolution of initial energy distribution among different gravity waves. After these works, a vast amount of research was carried out on wave interactions among geophysical waves, such as water waves and currents in deep water and shallow water [22,23], ocean surface waves [24], Rossby waves [25,26], and solitary waves [27], to name a few. From previous studies based on the perturbation expansion [19–21,24,25], the energy distribution is due to higher-order resonant wave interactions, which arise when the wave vectors and frequencies of the interacting waves satisfy the same functional relationship.

Various kinds of nonlinear interactions are involved in energy exchange among internal waves that are important to understand the instabilities and mixing processes in the ocean. A specific class of such interaction mechanisms in the context of oceanic internal waves is resonant triad interactions (RTIs). RTIs involve three waves whose wave vectors and frequencies satisfy the spatial and temporal resonance conditions, namely, $\vec{k}_3 = \pm\vec{k}_1 \pm \vec{k}_2$ and $\omega_3 = \pm\omega_1 \pm \omega_2$, where $\vec{k}_{1,2,3}$ and $\omega_{1,2,3}$ are the wave vectors and frequencies of the interacting waves; see [7] and references therein. A special type of RTI in internal waves is the triadic resonance instability (TRI) [7,28,29] in which a primary wave—forming a resonant triad with a pair of secondary waves of smaller frequencies—becomes unstable, resulting in the transfer of energy from the primary wave to the secondary waves.

To understand the nonlinear effects on the stability of internal waves forming a resonant triad, it is customary to use the amplitude equations [30–34]. In practice, the amplitude equations are derived and solved to track the nonlinear evolution of the amplitudes of the waves forming a resonant triad. Note that the amplitude equations are derived under the assumption of small but finite amplitude waves and are valid in the weakly nonlinear regime. In an inviscid fluid, a criterion for the stability of a resonant triad formed by one primary internal wave of finite amplitude and a pair of secondary internal waves of infinitesimal amplitudes was given by Hasselmann [35], which assumes that the primary wave has the highest frequency in the triad. Under the above conditions, a triad is unstable when $\vec{k}_1 + \vec{k}_2 = \vec{k}_3$ and $\omega_1 + \omega_2 = \omega_3$. Here, $(\vec{k}_{1,2}, \omega_{1,2})$ and $(\vec{k}_3, \omega_3)$, $\omega_{1,2,3} > 0$ represent the wave vector and frequency pairs of the infinitesimal and finite components of the triad, respectively. The assumption wherein the initial amplitude of one of the waves in a triad is much larger than the amplitudes of other two waves is known as the pump-wave approximation, and the wave with the largest amplitude is referred to as the pump wave [31,35]. In this approximation, the effect of the waves with smaller amplitudes on the pump wave is neglected, and the amplitude of the pump wave is treated as a constant. In the case of RTIs among internal waves, the growth rates of the secondary internal waves are maximum when $\omega_1 = \omega_2 = \omega_3/2$, and $|\vec{k}_1|, |\vec{k}_2| \gg |\vec{k}_3|$; due to this instability, energy transfer occurs from the long internal wave to short internal waves [7]. Under the pump-wave approximation, Craik *et al.* [31] presented and analyzed some exact solutions of the amplitude equations wherein the amplitude was assumed to be a slowly varying function of both space and time. In a subsequent study, Craik and Stewartson [30] discussed a class of exact solutions of the amplitude equations for RTIs, which deals with the bursting of localized perturbations in the case of RTIs.

Within the framework of the amplitude equations, several studies [17,34,36,37] have been carried out to understand RTIs arising in different variants of stratified flows. Notably, in the absence of any background shear, RTIs among three internal waves having three distinct mode numbers in continuously stratified fluids was discussed by Thorpe [38]. He presented an analytical relationship among the mode numbers and frequencies of the waves present in the resonant triad. Grimshaw [34] studied the local evolution of the RTIs of internal waves originating from a stratified shear flow through the slowly varying amplitude equations. The present work closely follows and extends Thorpe's work [38] by including a background shear and focuses on the uniformly stable stratification (i.e., density decreases uniformly with the height). Following the approach of the amplitude equation, in the present study, we investigate a nonlinear wave interaction forming a resonant triad in an inviscid stratified uniform shear flow.

The main objectives of the present work are to derive the weakly nonlinear amplitude equations for RTIs arising in a uniformly stratified shear flow and to analyze the stability of resonant triads. In particular, we focus on RTIs in which two primary waves of frequency $\omega$ interact and produce a superharmonic wave. To understand the evolution of amplitudes of the resonant waves, we solve the coupled amplitude equations numerically. We present the analytical solution of amplitude equations under the pump-wave approximation by assuming a primary wave of the lowest mode number as the pump wave. We shall illustrate the stability of resonant triads for different local Richardson numbers from the temporal behavior of the amplitudes of the internal waves involved in the triad, starting from different initial values. The stability of such solutions of amplitude equations is crucial for understanding the stability of a resonant triad, and hence the energy transfer mechanism among waves in a resonant triad.

Here we identify the aforementioned resonant triads arising in a stably stratified uniform shear flow. Although other studies [34,38] have approached similar problems, the effect of background shear flow on RTIs among two primary and one superharmonic modes is still poorly understood. For instance, it is unclear how the presence of uniform shear in a stratified flow affects the formation of resonant triads among three different modes and the evolution of their amplitudes. For more realistic scenarios, one needs to consider the effect of viscosity, diffusivity, and Earth's rotation on triad interactions. The inclusion of such effects on the RTIs of internal waves is far beyond the scope of the present study and will be considered elsewhere in the future.

The paper is organized as follows. In Sec. II, the description of the problem, governing equations, and details of the disturbance equations are presented. The analytical solution of the linear problem and the existence of RTIs are demonstrated in Sec. III. The formulation of the nonlinear problem consisting of the adjoint problem is outlined in Sec. IV A. The amplitude equations for the problem under consideration are derived in Sec. IV B. The equilibrium solutions and their linear stability are discussed in Sec. IV C. The exact solution under the pump-wave approximation is analyzed in Sec. V. At the end, conclusions are given in Sec. VI.

## II. PROBLEM FORMULATION

Let us consider a two-dimensional parallel shear flow driven by two oppositely moving horizontal plates with speed $U_p$ located at $z = \pm H$. Here, $x$ and $z$ are the streamwise (horizontal) and transverse (vertical) directions, respectively. The basic flow assumes unperturbed velocity $U = U_p z/H$ and density profile $\bar{\rho}(z)$ with pressure $P(z)$. We also assume that the shear is uniform (i.e., overall shear rate $U_p/H$ is a constant) and that the density profile is linearly stably stratified [i.e., $\bar{\rho}(z) \propto -z$]. The total velocity, pressure, and density fields are indicated here, which are decomposed into the basic (or unperturbed) flow fields plus the perturbation fields as $(U + u, w)$, $P + p$, and $\bar{\rho} + \rho$, respectively, where the perturbations $u$, $w$, $p$, and $\rho$ may depend on the horizontal $x$ and vertical $z$ directions and the time $t$. Under the Boussinesq approximation, in which the density variations can be neglected in the inertial term, the balance equations for the mass, energy, and momentum

reduce to

$$\partial_x(U+u)+\partial_z w=0, \tag{1}$$

$$\partial_t(\bar{\rho}+\rho)+(U+u)\partial_x(\bar{\rho}+\rho)+w\partial_z(\bar{\rho}+\rho)=0, \tag{2}$$

$$\partial_t(U+u)+(U+u)\partial_x(U+u)+w\partial_z(U+u)=-\frac{1}{\varrho_m}\partial_x(P+p), \tag{3}$$

$$\partial_t w+(U+u)\partial_x w+w\partial_z w=-\frac{g}{\varrho_m}(\bar{\rho}+\rho)-\frac{1}{\varrho_m}\partial_z(P+p), \tag{4}$$

where $\partial_t \equiv \partial/\partial t$, $\partial_x \equiv \partial/\partial x$, and $\partial_z \equiv \partial/\partial z$ denote the partial derivatives with respect to $t$, $x$, and $z$, respectively, and $\varrho_m$ is a constant background density. Since $\partial_x U=\partial_x\bar{\rho}=\partial_x P=0$ and $g\bar{\rho}/\varrho_m+\partial_z P/\varrho_m=0$, we get

$$\partial_x u+\partial_z w=0, \tag{5}$$

$$(\partial_t+U\partial_x)\rho+w\,\partial_z\bar{\rho}=-(u\,\partial_x\rho+w\,\partial_z\rho), \tag{6}$$

$$(\partial_t+U\partial_x)u+w\partial_z U=-(u\,\partial_x u+w\,\partial_z u)-\frac{1}{\varrho_m}\partial_x p, \tag{7}$$

$$(\partial_t+U\partial_x)w=-(u\,\partial_x w+w\,\partial_z w)-\frac{g}{\varrho_m}\rho-\frac{1}{\varrho_m}\partial_z p. \tag{8}$$

Eliminating the pressure from (7) and (8), replacing the base state density gradient from the left-hand side of (6) by the squared buoyancy frequency $N^2$ defined as $N^2=-g/\varrho_m\partial_z\bar{\rho}$, and introducing the perturbed stream function $\psi(x,z,t)$ with $(u,w)=(\partial_z\psi,\ -\partial_x\psi)$, we get the following equations:

$$(\partial_t+U\partial_x)\rho+\frac{\varrho_m N^2}{g}\partial_x\psi=J(\psi,\rho), \tag{9}$$

$$(\partial_t+U\partial_x)\nabla^2\psi-(\partial_x\psi)(\partial_{zz}U)=\frac{g}{\varrho_m}\partial_x\rho+J(\psi,\nabla^2\psi), \tag{10}$$

where $\nabla^2$ denotes the Laplacian and $J$ is the Jacobian determinant. In general, the buoyancy frequency $N$ depends on the vertical coordinate $z$, e.g., in the ocean, $N$ is larger in the thermocline than in the abyss. Here, we study the uniform shear flow with stable stratification, i.e., $N^2>0$. We also assume a constant buoyancy frequency, which implies uniform stratification throughout the flow domain.

For nondimensionalization, we choose the reference scales for density, velocity, length, time, and buoyancy frequency as $\varrho_m$, $U_p$, $H$, $H/U_p$, and $\sqrt{g/H}$, respectively. Using this scaling and a further simplification that $U$ varies linearly with $z$, the dimensionless equations read

$$(\partial_t+U\partial_x)\rho+N^2\partial_x\psi=J(\psi,\rho), \tag{11}$$

$$(\partial_t+U\partial_x)\nabla^2\psi=\mathrm{Ri}_0\,\partial_x\rho+J(\psi,\nabla^2\psi), \tag{12}$$

where $\mathrm{Ri}_0=gH/U_p^2$ is the (dimensionless) bulk Richardson number and $N$ is the dimensionless buoyancy frequency. For simplicity, the same notations are kept in Eqs. (11) and (12) for the nondimensional variables and the parameter $N$. Furthermore, we assume no-slip and zero density perturbation conditions at the boundaries $z=\pm1$.

## III. LINEAR PROBLEM: NORMAL MODE SOLUTION

In this section, we perform the linear stability of the base flow subject to infinitesimal perturbations. For this, we neglect the nonlinear perturbation terms of (11) and (12) to get linearized

perturbation equations,

$$(\partial_t + U\partial_x)\rho + N^2\partial_x\psi = 0 \quad \text{and} \quad (\partial_t + U\partial_x)\nabla^2\psi - \mathrm{Ri}_0\,\partial_x\rho = 0. \tag{13}$$

Since the linear equations (13) are transnational invariant in $x$ and $t$, we can assume a normal mode solution for the perturbation variables,

$$(\psi,\ \rho) = [\hat{\psi}(z),\ \hat{\rho}(z)]\, e^{ik(x-ct)}, \tag{14}$$

where $k$ is the real horizontal wave number, $c = c^{(r)} + ic^{(i)}$ is the complex phase velocity with superscripts $(r)$ and $(i)$ denoting the real and imaginary parts, and $\hat{\psi}(z)$ and $\hat{\rho}(z)$ represent $z$-dependent amplitudes of the perturbed stream function and perturbed density, respectively, which can be complex-valued functions. The linear stability of the base flow is determined by the sign of the imaginary part of the complex phase velocity $c$; the flow is stable, unstable, or neutrally stable if $c^{(i)} < 0$, $c^{(i)} > 0$, or $c^{(i)} = 0$, respectively. Substituting (14) into (13), we get the following generalized matrix eigenvalue problem:

$$\mathcal{L}X = c\mathcal{M}X, \tag{15}$$

where

$$\mathcal{L} = \begin{bmatrix} U(D^2 - k^2) & -\mathrm{Ri}_0 \\ N^2 & U \end{bmatrix}, \quad \mathcal{M} = \begin{bmatrix} D^2 - k^2 & 0 \\ 0 & 1 \end{bmatrix}, \quad D = \frac{d}{dz}, \quad \text{and} \quad X = \begin{bmatrix} \hat{\psi} \\ \hat{\rho} \end{bmatrix}. \tag{16}$$

The resulting eigenvalue problem (15) and (16), along with the boundary conditions $\hat{\rho} = \hat{\psi} = 0$ at $z = \pm 1$, is solved numerically using the Chebyshev spectral collocation method [39].

For long-wave (i.e., $k = 0$) perturbations, the eigenvalues of the linearized system have been determined in terms of the hyperbolic functions [16,40],

$$c_j(\mathrm{Ri}) = \coth\left(\frac{j\pi}{2\sqrt{\mathrm{Ri} - 0.25}}\right), \quad j = 1, 2, 3, \ldots, \quad \mathrm{Ri} > 0.25, \tag{17}$$

where $\mathrm{Ri} = \mathrm{Ri}_0 N^2$ is the local Richardson number, which represents the local gradient of background density. Due to the uniform stratification ($N$ = constant), the local Richardson number remains constant in the present problem. Note that to find the parameters for which resonant triad interactions (RTIs) exist, one needs to find a set of wave numbers and frequencies satisfying the dispersion relation, which is explained in Sec. III A.

### A. Analytical solution

The linearized problem (15) admits an analytical solution in terms of the modified Bessel functions [41,42]. To find the analytical solution of (15), we eliminate density, which yields the simplified version of the well-known Taylor-Goldstein equation,

$$[(U - c)^2(D^2 - k^2) + \mathrm{Ri}]\hat{\psi} = 0, \tag{18}$$

where $U = z$, $\forall z$, $z \neq c$ in order to avoid singularity. Here, we fix the local Richardson number greater than 0.25 to ensure the existence of an infinite number of discrete eigenvalues of (15) as well as the linear stability of the stratified flow [14]. Note that (18) can be transformed to the modified Bessel equation [40] as

$$\hat{\psi}(z) = [k(z - c)]^{1/2}\{K_\nu[k(-1 - c)]I_\nu[k(z - c)] - I_\nu[k(-1 - c)]K_\nu[k(z - c)]\}, \tag{19}$$

where $z \neq c$, and $I_\nu$ and $K_\nu$ are the modified Bessel functions of the order of $\nu = (0.25 - \mathrm{Ri})^{1/2}$. Here, $\nu$ is a purely imaginary number as $\mathrm{Ri} > 0.25$, which also assures neutrally stable modes in the system. By employing the boundary conditions, we get the dispersion relation relating the frequency

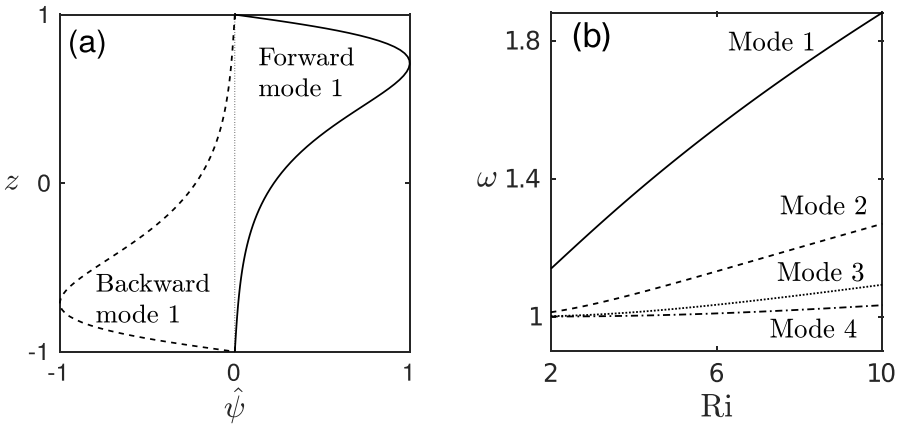


FIG. 1. (a) The forward and backward propagating mode 1, $\hat{\psi}(z)$, for $\mathrm{Ri} = 8.2$ and $k = 3.599$ with frequencies $\omega = 4.51$ and $-4.51$, respectively. $\hat{\psi}(z)$ is normalized in such a way that $\max_{z\in[-1,1]} |\hat{\psi}(z)| = 1$. (b) Variation of frequency $\omega$ of different forward modes (mode 1 to mode 4) of wave number $k = 1$ with the local Richardson number Ri, where the solid, dashed, dotted, and dash-dotted lines represent the frequencies of mode 1 to mode 4, respectively.

($\omega = kc$) and the wave number ($k$) as

$$\mathcal{D}(k,\omega) = \begin{vmatrix} I_\nu(-k-\omega) & K_\nu(-k-\omega) \\ I_\nu(k-\omega) & K_\nu(k-\omega) \end{vmatrix} = 0. \tag{20}$$

By solving dispersion relation (20) empirically for different local Richardson number, an infinite set of wave numbers at a fixed frequency as well as an infinite set of frequencies at a fixed wave number are obtained. Note that as the flow domain is vertically bounded, the waves appearing in the flow are confined in a finite-depth region between the plates at $z = \pm 1$; therefore, one can describe such waves in terms of different modes. These different modes at a particular frequency $\omega$ having wave numbers $k_1, k_2, k_3, \ldots$ are arranged in ascending order of their wave numbers, i.e., $k_1 < k_2 < k_3 \cdots$; these modes are referred to as the first mode, second mode, third mode, and so on. It is clear from the relation $\omega = k_i c_i$ that for a fixed frequency $\omega$, as the mode number increases, the phase speed $c_i$ decreases, and thus the first mode has the maximum phase speed, i.e., the first mode is the fastest traveling mode.

It is verified that the numerically obtained eigenvalues from (15) match excellently with those obtained by solving (20) analytically. In the present study, we observe that the growth rates are zero, and hence all the modes are neutrally stable (i.e., $c = c^{(r)}$ and $\omega = \omega^{(r)} = kc^{(r)}$ are real). This is expected from the choice of the local Richardson number $\mathrm{Ri} > 0.25$ [19]. The discrete modes present in the system can be classified into two categories depending on their phase speeds, namely, the forward ($c = c^{(r)} > 1$, $\omega = \omega^{(r)} > k$) and backward ($c = c^{(r)} < -1$, $\omega = \omega^{(r)} < -k$) propagating modes. Physically, the forward (backward) propagating mode travels faster (slower) than the background shear flow without altering its stability.

Figure 1(a) depicts the forward propagating mode 1 ($\omega = 4.51$) and the backward propagating mode 1 ($\omega = -4.51$) for $\mathrm{Ri} = 8.2$ and $k = 3.599$. It has been found [but shown only for mode 1 in Fig. 1(a)] that for every forward propagating mode $\hat{\psi}(z)$ having frequency $\omega$, there exists a backward propagating mode $-\hat{\psi}(-z)$ having frequency $-\omega$. In other words, the forward and backward propagating modes have symmetry about the origin in the $(\hat{\psi}, z)$ plane. Therefore, in what follows, we shall consider only the forward propagating modes; a similar analysis for the backward propagating modes can be carried out analogously. For wave number $k = 1$, the variation of frequencies of the first four forward propagating modes with the local Richardson number Ri

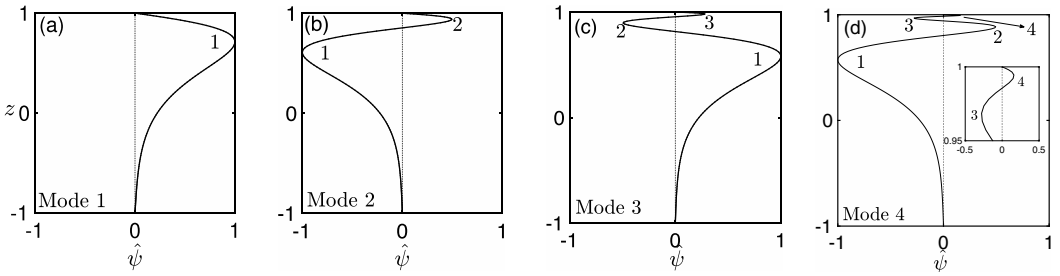


FIG. 2. First four forward propagating modes for $\omega = 4.51$ and $\mathrm{Ri} = 8.2$, where numbers near the curves represent the counting of local extrema. The wave numbers $k_1$ to $k_4$ for mode 1 to mode 4 are 3.59903, 4.506, 4.50996, 4.50998, respectively. The inset in (d) shows a zoomed portion near the third and fourth local extrema.

is presented in Fig. 1(b). Here, the bulk Richardson number $\mathrm{Ri}_0$ is specified as 1. It is clear that the frequency of each mode is a strictly increasing function of Ri, and the rate of change of the frequency is maximum for mode 1. As the mode number increases, the frequency increases slowly with Ri. Physically, the frequency of the mode having the maximum phase speed increases most rapidly with the squared natural frequency of the vertical oscillation of the fluid, i.e., $N^2$, since $\mathrm{Ri}_0$ is a constant. In other words, increasing the buoyancy frequency leads to high-frequency waves in the system.

The first four forward propagating modes having frequency $\omega = 4.51$ for $\mathrm{Ri} = 8.2$ are illustrated in Fig. 2. It is evident from Fig. 2 that a mode structure depends on its mode number because the number of extrema of a mode inside the flow domain is equal to the mode number. It is worth noting that in the absence of background shear flow, the vertical structures of the internal modes are simply the sine and cosine functions [8]. However, in the presence of shear, the vertical structures of these modes turn out as the modified Bessel functions (19). In what follows, the symmetry of the mode structures breaks down due to (uniform) shear flow; see Fig. 2.

Figure 3(a) illustrates the variation of frequency of the first and third forward propagating modes with the wave number; the other parameters are the same as those in Fig. 2. It is seen that the frequency of each mode increases with the wave number. The wave number and frequency pairs of the waves forming a resonant triad, listed in the first row of Table I, are marked with circles; see

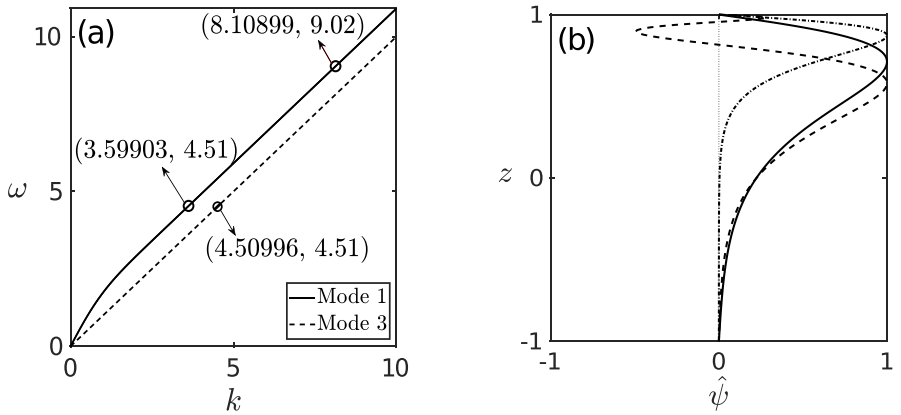


FIG. 3. (a) Variation of frequency with the wave number for the first (solid line) and third (dashed line) modes, where the circle denotes the wave number and frequency pairs of the waves forming a resonant triad. (b) Variation of two primary modes (solid and dashed lines) and a secondary mode (dot-dashed line). Other parameters are the same as in Fig. 2.

TABLE I. The parameters associated with resonant triad interactions among waves with mode numbers $m$, $n$, and $r$ in a stably stratified uniform shear flow.

| (m,n) | Ri | $\omega$ | $k_m$ | $k_n$ | $k_m + k_n$ | $k_r$ | $2\omega$ | $\omega_r$ | $\lvert 2\omega - \omega_r \rvert$ |
|---|---|---|---|---|---|---|---|---|---|
| (1,3) | 8.2 | 4.51 | 3.59903 | 4.50996 | 8.10899 | 8.10899 | 9.02 | 9.02000 | $9.2455 \times 10^{-7}$ |
| (1,4) | 7.3 | 4.21 | 3.39878 | 4.20994 | 7.60872 | 7.60872 | 8.42 | 8.42000 | $5.2173 \times 10^{-8}$ |
| (2,3) | 6.7 | 4.21 | 4.20482 | 4.20956 | 4.41438 | 8.41482 | 8.42 | 8.41998 | $1.1682 \times 10^{-5}$ |
| (2,4) | 2.2 | 1.81 | 1.79103 | 1.80979 | 3.60082 | 3.60081 | 3.62 | 3.62000 | $7.9970 \times 10^{-7}$ |
| (3,4) | 2.0 | 2.61 | 2.60865 | 2.60987 | 5.21852 | 5.21865 | 5.22 | 5.2200 | $6.4018 \times 10^{-8}$ |

next section for more detail. It is found that at frequency $\omega = 4.51$, mode 1 and mode 3 give rise to a secondary wave with frequency $\omega = 9.02$ (see the next section for more details). Indeed, this secondary wave is a mode 1 of double frequency as its wave number and frequency pair satisfies the dispersion relation (top circle lying on the solid line) along with the mode boundary conditions; see the variation of the mode shown by the dash-dotted line in Fig. 3(b). These three interacting modes, depicted by circles in Fig. 3(a), are illustrated in Fig. 3(b). The secondary mode (dash-dotted line) satisfies the dispersion relation and boundary conditions. Note that the secondary mode carries mode number 1 and has a shorter wavelength than primary mode 1 (solid line).

Similarly to Fig. 3, for other interacting wave pairs, one can check whether or not a secondary wave generated by the resonant triad interaction of two primary modes is a mode. If a secondary wave satisfies the dispersion relation as well as the mode boundary conditions, then it is a mode. In order to verify that the secondary wave satisfies the mode boundary conditions, one needs to verify the spatial structure of the wave having the same wave number and frequency as the secondary wave.

### B. Evidence of resonant triad interactions

In general, three waves form a resonant triad if their wave vectors ($\vec{k}_1,\ \vec{k}_2,\ \vec{k}_3$) and frequencies ($\omega_1,\ \omega_2,\ \omega_3$) satisfy the following conditions:

$$\vec{k}_3 = \pm\vec{k}_1 \pm \vec{k}_2 \quad \text{and} \quad \omega_3 = \pm\omega_1 \pm \omega_2. \tag{21}$$

The wave vector in the present problem is one dimensional [see (14)], i.e., $(|\vec{k}_1|, |\vec{k}_2|, |\vec{k}_3|) = (k_1, k_2, k_3)$, with $k_{1,2,3}$ being the wave numbers along the $x$ direction. In the present paper, we focus on a special type of resonant triad, where two primary waves of different wave numbers $k_1 = k_m$ and $k_2 = k_n$ having the same frequency $\omega_1 = \omega_2 = \omega$ interact and produce the secondary wave of frequency $\omega_3 = 2\omega$ and wave number $k_3 = k_m + k_n$; thus satisfying conditions $k_3 = k_1 + k_2$ and $\omega_3 = \omega_1 + \omega_2$. Here, the subscripts $m$ and $n$ denote the mode numbers of the primary waves (see Sec. III A). Since the present flow configuration is vertically bounded, the primary waves are described as modes. Usually, the secondary wave is not compelled to be a mode. However, for the interaction cases considered here, the secondary waves are turned out as modes; see Fig. 4 and Table II for more detail. To search for parameter space pertaining to a resonant triad, we solve the dispersion relation (20) by appropriately choosing the range of $\omega$ and Ri. For each pair of $\omega$ and Ri, the dispersion relation (20) is solved for $k$. Hence, the obtained wave numbers $k$ can be arranged in ascending order, $k_1 < k_2 < k_3 < k_4 \cdots$. Once again, we solve (20) for finding frequencies $\omega$ at fixed $k = k_m + k_n$ and Ri, where $k_m$ and $k_n$ are the wave numbers obtained from the previous calculations. From these calculations, we get countably many $\omega$ satisfying the dispersion relation $\mathcal{D}(k_m + k_n, \omega) = 0$, among which we pick a particular solution, say $\omega_r$, such that $2\omega = \omega_r$. Owing to the computational limitations, $2\omega$ can never be exactly equal to $\omega_r$; however, the absolute difference $|2\omega - \omega_r|$ can be made arbitrarily small, which determines the strength of a resonant triad. The existence of a resonance triad is confirmed if the condition $|2\omega - \omega_r| = 0$ is satisfied

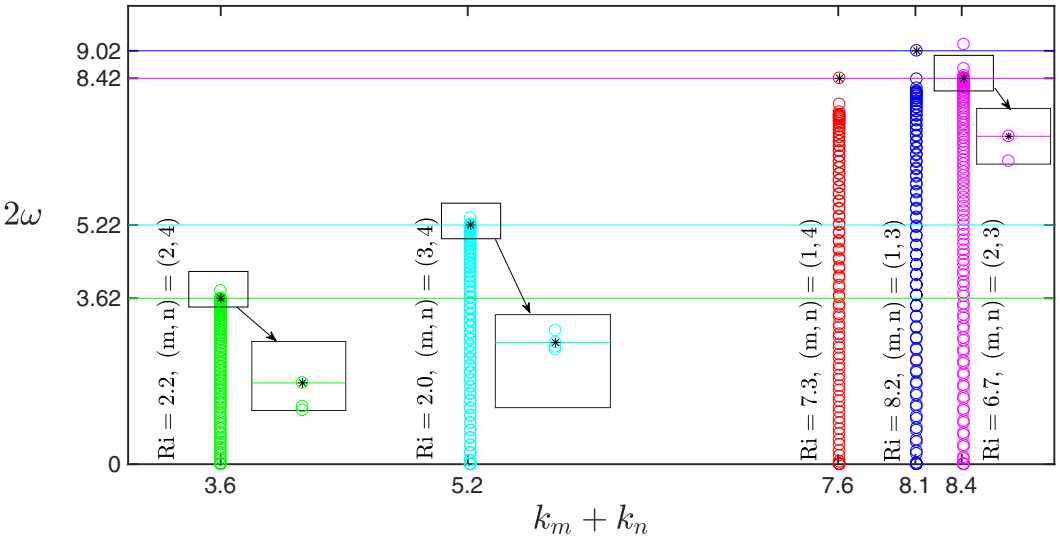


FIG. 4. Graphical representation of the resonant triad condition for the parameters listed in Table I. Vertically aligned circles represent the eigenvalues of the linear problem at wave number $k_m + k_n$ (sixth column of Table I). The horizontal lines depict $2\omega$ (eighth column of Table I) corresponding to each $(m, n)$. The points $(k_m + k_n, 2\omega)$ are marked by black stars. Insets show the zoomed portion of those parts where a circle is overlapping with a star.

with some specified accuracy, i.e., $|2\omega - \omega_r| \approx 0$. By testing this condition, we get parameters $\omega$ and Ri leading to strong resonant triads. For a few pairs of different mode numbers such that $1 \leqslant m \leqslant 4$ and $1 \leqslant n \leqslant 4$ with $m < n$, Table I summarizes the values of the parameters at which $|2\omega - \omega_r| \approx 0$, thereby leading to strong resonance triads.

The existence of resonant triad interactions (RTIs) in the present system is represented graphically in Fig. 4. All possible frequencies for the modes corresponding to the wave number $k = k_m + k_n$ are shown in Fig. 4, where $k_m$ and $k_n$ are chosen from the fourth and fifth columns of Table I. The same color circles in Fig. 4 represent the frequencies at fixed Ri and fixed pair of mode numbers $(m, n)$. For reference, the frequencies listed in the eighth column of Table I are shown by the horizontal lines. The intersection of a circle and a horizontal line, marked with a (black) star, represents the point $(k_m + k_n, 2\omega)$ at which RTIs appear. It is evident that in each case, the number $2\omega$ (star) matches exactly with one of the frequencies $\omega_r$ at wave number $k = k_m + k_n$. Consequently, there exists a primary mode with frequency $2\omega$ at wave number $k_m + k_n$, and hence conditions (21) of a resonant triad are satisfied exactly for the considered parameter values (listed in Table I).

TABLE II. The wave numbers of modes at frequency $2\omega$ for different Ri. The wave numbers in bold represent the wave numbers of the superharmonic wave generated by the interaction of two primary waves of frequency $\omega$ and wave numbers $k_m$ and $k_n$ as listed in Table I.

| Ri | $2\omega$ | $k_1$ | $k_2$ | $k_3$ | $k_4$ | $k_5$ | $k_6$ |
|---|---|---|---|---|---|---|---|
| 8.2 | 9.02 | **8.10899** | 8.92412 | 8.98854 | 9.00968 | 9.01661 | 9.01889 |
| 7.3 | 8.42 | **7.60872** | 8.17609 | 8.34542 | 8.39716 | 8.413 | 8.41786 |
| 6.7 | 8.42 | 7.67696 | 8.20797 | 8.35854 | 8.40216 | **8.41482** | 8.4185 |
| 2.2 | 3.62 | 3.43751 | **3.60081** | 3.61798 | 3.61979 | 3.61998 | 3.62 |
| 2.0 | 5.22 | 5.0635 | 5.20547 | **5.21865** | 5.21987 | 5.21999 | 5.22 |

For more clarity, we solve dispersion relation (20) by replacing the frequency $\omega$ in (20) with the values listed in the sixth column of Table I (corresponding to $2\omega$) to determine the associated wave numbers, which are displayed in Table II. Clearly, each value of $k_m + k_n$ listed in the eighth column of Table I appears in each corresponding row of Table II; see the bold cells in Table II (note that the wave numbers in each row of Table II are sorted in ascending order). Thus the existence of a secondary mode with wave number $k_m + k_n$ and frequency $2\omega$ is also confirmed from Table II. Moreover, the mode number of the secondary wave, resulting from the interaction of two primary waves, can be determined from Table II. For instance, the mode number of the secondary wave is equal to two for the parameters corresponding to the fourth row.

In the no-shear case, Thorpe [38] derived an explicit expression for the existence of RTIs,

$$\frac{\omega}{N^2} = \frac{(3m-n)(3n-m)}{16mn}, \tag{22}$$

where $m$, $n$, and $\omega$ are the mode numbers and frequency of two primary waves of a triad, respectively. Further, he found that the mode number of the superharmonic wave, forming a resonant triad with these two waves, is equal to $|m-n|$. Consequently, for a given buoyancy frequency $N$, we can easily examine whether or not the mode $m$ and mode $n$ at frequency $\omega$ lead to a resonant triad. For instance, RTIs are not possible when forward propagating modes with $(m, n) = (1, 3)$ and (1,4) at any given frequency $\omega$ interact. In the presence of shear flow, no such analytical expression relating the mode numbers and frequency of the interacting waves exists for RTIs. In this case, the only way to calculate the mode number of the superharmonic mode is to count the number of local extrema in their vertical structures. In the next section, we investigate the nonlinear problem, where we derive the amplitude equations for the waves forming RTIs.

## IV. NONLINEAR PROBLEM

### A. Adjoint problem and biorthogonality relation

To derive the amplitude equations, one requires the orthogonality relation between the regular and adjoint eigenfunctions that can be obtained as follows. We first define an inner product,

$$\langle \mathcal{L}X,\ X^\dagger \rangle = \int_{-1}^{1} X^{\dagger *} \mathcal{L}X\, dz = \int_{-1}^{1} (\mathcal{L}^\dagger X^\dagger)^* X dz = \langle X,\ \mathcal{L}^\dagger X^\dagger \rangle, \tag{23}$$

where $\mathcal{L}^\dagger$ and $X^\dagger = (\xi, \eta)^T$ denote the adjoint operator and the adjoint eigenfunction, respectively, and the superscript $*$ denotes the conjugate transpose. By employing a few steps of integration by parts and applying the boundary conditions, we obtain the adjoint operator $\mathcal{L}^\dagger$ associated with the linear operator $\mathcal{L}$ as

$$\mathcal{L}^\dagger = \begin{bmatrix} U(D^2 - k^2) + 2U'D & N^2 \\ -\mathrm{Ri}_0 & U \end{bmatrix}. \tag{24}$$

Recall that the operator $\mathcal{M}$ is a self-adjoint operator, and thus the adjoint problem takes the following form:

$$\mathcal{L}^\dagger X^\dagger = c^*\, \mathcal{M} X^\dagger \quad \text{with} \quad \xi = \eta = 0 \quad \text{at} \quad z = \pm 1. \tag{25}$$

It is well known that the eigenvalues of the adjoint problem (25) are the complex conjugate of the eigenvalues of the regular problem (15). In the present problem, all eigenvalues of the regular problem are real and, therefore, $c = c^*$.

To derive the orthogonality relation, we rewrite (23) as

$$\int_{-1}^{1} [X_j^{\dagger *} \mathcal{L}_i X_i - (\mathcal{L}_j^\dagger X_j^\dagger)^* X_i] dz = 0, \tag{26}$$

where $\mathcal{L}_i = \mathcal{L}(k \to k_i)$ and $\mathcal{L}_j^\dagger = \mathcal{L}^\dagger(k \to k_j)$. Here, the notations $\mathcal{L}(k \to k_i)$ and $\mathcal{L}^\dagger(k \to k_j)$ imply that the wave numbers $k$ in the operators $\mathcal{L}$ and $\mathcal{L}^\dagger$, defined in (16) and (24), are replaced by the wave numbers $k_i$ of the $i$th mode and $k_j$ of the $j$th mode, respectively. Substituting $\mathcal{L}_i X_i$ and $\mathcal{L}_j^\dagger X_j^\dagger$ from (15) and (25) into (26), we obtain

$$c_i \int_{-1}^{1} X_j^{\dagger *} \mathcal{M}_i X_i dz - c_j^* \int_{-1}^{1} (\mathcal{M}_j X_j^\dagger)^* X_i dz = 0,$$

where $\mathcal{M}_i = \mathcal{M}(k \to k_i)$ and $\mathcal{M}_j = \mathcal{M}(k \to k_j)$. Applying integration by parts in the second term of the above equation, we obtain

$$(c_i - c_j^*) \int_{-1}^{1} X_j^{\dagger *} \mathcal{M}_i X_i dz = 0, \tag{27}$$

which can also be written as

$$\int_{-1}^{1} X_j^{\dagger *} \mathcal{M}_i X_i dz = C\delta_{ij} \quad \text{or} \quad \langle \mathcal{M}_i X_i, X_j^\dagger \rangle = C\delta_{ij}, \tag{28}$$

where $\delta_{ij}$ is the Kronecker delta. The regular and adjoint eigenfunctions can be normalized such that $C = 1$.

### B. Derivation of the amplitude equations

In this section, we derive the amplitude equations when the two primary waves interact with the superharmonic wave and form a resonant triad [17,43]. Note that the amplitude equations are strictly valid in the weakly nonlinear region, i.e., close to the linear stability threshold. Nevertheless, in fully nonlinear regimes, these equations can provide qualitative information about the underlying physics. It is worth mentioning that the amplitude equations are independent of the choice of a physical system, and that the coefficients of the amplitude equations are enough to know the growth or decay of a weakly nonlinear perturbation.

To derive the amplitude equations for resonant triad interactions, we assume the normal mode expansion in a general form,

$$(\psi, \rho) = \sum_j [\hat{\psi}_j(z), \hat{\rho}_j(z)] A_j(t) E_j, \tag{29}$$

where $A_j$'s are the algebraic time-dependent amplitudes of the $j$th wave, and $E_j = e^{ik_j(x - c_j t)}$. Substituting (29) with only three modes $j \in \{m, n, r\}$ into (12) and collecting the coefficients of $E_m$, $E_n$, and $E_r$, we get

$$\begin{aligned}
\left(\frac{dA_m}{dt} - ik_m c_m A_m\right) \begin{bmatrix} D^2 - k_m^2 & 0 \\ 0 & 1 \end{bmatrix} \begin{bmatrix} \hat{\psi}_m \\ \hat{\rho}_m \end{bmatrix} &= A_n^*(t) A_r(t) f_m(z), \\
\left(\frac{dA_n}{dt} - ik_n c_n A_n\right) \begin{bmatrix} D^2 - k_n^2 & 0 \\ 0 & 1 \end{bmatrix} \begin{bmatrix} \hat{\psi}_n \\ \hat{\rho}_n \end{bmatrix} &= A_m^*(t) A_r(t) f_n(z), \\
\left(\frac{dA_r}{dt} - ik_r c_r A_r\right) \begin{bmatrix} D^2 - k_r^2 & 0 \\ 0 & 1 \end{bmatrix} \begin{bmatrix} \hat{\psi}_r \\ \hat{\rho}_r \end{bmatrix} &= A_m(t) A_n(t) f_r(z).
\end{aligned} \tag{30}$$

Here, $f_m(z)$, $f_n(z)$, and $f_r(z)$ are the nonlinear terms,

$$
\begin{aligned}
f_m(z) &= \begin{bmatrix} f_{m1}(z) \\ f_{m2}(z) \end{bmatrix} = \begin{bmatrix} J(\hat{\psi}_r, \hat{\psi}_n^*) + J(\hat{\psi}_n^*, \hat{\psi}_r) \\ J(\hat{\psi}_r, \hat{\rho}_n^*) + J(\hat{\rho}_n^*, \hat{\psi}_r) \end{bmatrix}, \\
f_n(z) &= \begin{bmatrix} f_{n1}(z) \\ f_{n2}(z) \end{bmatrix} = \begin{bmatrix} J(\hat{\psi}_r, \hat{\psi}_m^*) + J(\hat{\psi}_m^*, \hat{\psi}_r) \\ J(\hat{\psi}_r, \hat{\rho}_m^*) + J(\hat{\rho}_m^*, \hat{\psi}_r) \end{bmatrix}, \\
f_r(z) &= \begin{bmatrix} f_{r1}(z) \\ f_{r2}(z) \end{bmatrix} = \begin{bmatrix} J(\hat{\psi}_m, \hat{\psi}_n) + J(\hat{\psi}_n, \hat{\psi}_m) \\ J(\hat{\psi}_m, \hat{\rho}_n) + J(\hat{\rho}_n, \hat{\psi}_m) \end{bmatrix},
\end{aligned} \tag{31}
$$

where $J(\hat{\psi}_i, \hat{\psi}_j) = (ik_i\hat{\psi}_i)(M_jD\hat{\psi}_j) - (D\hat{\psi}_i)(ik_jM_j\hat{\psi}_j)$, $J(\hat{\psi}_i, \hat{\rho}_j) = (ik_i\hat{\psi}_i)(D\hat{\rho}_j) - (D\hat{\psi}_i)(ik_j\hat{\rho}_j)$, and $M_j = D^2 - k_j^2$. Multiplying (30) with the conjugate transpose of the corresponding adjoint eigenfunction from the left and integrating with respect to $z$ from $-1$ to 1, we get

$$
\begin{aligned}
\frac{dA_m}{dt} - i\omega_m A_m &= \lambda_m A_n^*(t) A_r(t), \\
\frac{dA_n}{dt} - i\omega_n A_n &= \lambda_n A_m^*(t) A_r(t), \\
\frac{dA_r}{dt} - i\omega_r A_r &= \lambda_r A_m(t) A_n(t),
\end{aligned} \tag{32}
$$

where $\lambda_m$, $\lambda_n$, and $\lambda_r$ are the complex coupled coefficients of the amplitude equations and are defined as

$$
\lambda_j = \frac{\int_{-1}^{1} [\xi_j^* \quad \eta_j^*] \begin{bmatrix} f_{j1}(z) \\ f_{j2}(z) \end{bmatrix} dz}{\int_{-1}^{1} [\xi_j^* \quad \eta_j^*] \begin{bmatrix} (D^2 - k_j^2) & 0 \\ 0 & 1 \end{bmatrix} \begin{bmatrix} \hat{\psi}_j \\ \hat{\rho}_j \end{bmatrix} dz} \quad \text{for} \quad j = m, n, r. \tag{33}
$$

It is numerically verified that for the parameters considered here, both the regular $(\hat{\psi}_j, \hat{\rho}_j)$ and adjoint $(\xi_j, \eta_j)$ eigenfunctions are purely imaginary, which further implies that $\lambda_j^* = -\lambda_j$, i.e., $\lambda_j$'s are purely imaginary numbers. Our goal is to study the evolution of RTIs, i.e., the evolution of the amplitudes of the three waves (two primary waves and one secondary wave) having the wave number and frequency pairs as $(k_m, \omega)$, $(k_n, \omega)$, and $(k_m + k_n, 2\omega)$. For such choices of wave number and frequency pairs, the coefficients of the linear terms in (32) become $\omega_m = \omega_n = \frac{1}{2}\omega_r = \omega$ and $k_r = k_m + k_n$. The coupling coefficients $\lambda_{m,n,r}$ are calculated from (33) and are listed in Table III for the parameters given in Table I. It is evident from Table III that the coefficients $\lambda_{m,n,r}$ of the amplitude equations (32) are purely imaginary.

With the known values of the coefficients of the amplitude equations, we analyze the solution of the amplitude equations (32), which is obtained numerically using the Runge-Kutta fourth-order

TABLE III. Coefficients of the amplitude equations for RTIs for various mode number pairs.

| (m,n) | Ri | $\omega$ | $k_m$ | $k_n$ | $\lambda_m$ | $\lambda_n$ | $\lambda_r$ |
|---|---|---|---|---|---|---|---|
| (1,3) | 8.2 | 4.51 | 3.59903 | 4.50996 | 2.58820 i | 0.01190i | −0.01463i |
| (1,4) | 7.3 | 4.21 | 3.39878 | 4.20994 | 2.77645i | 0.00745i | −0.32486i |
| (2,3) | 6.7 | 4.21 | 4.20482 | 4.20956 | −0.34448i | −0.02592i | −0.24006i |
| (2,4) | 2.2 | 1.81 | 1.79103 | 1.80979 | 0.16221i | 0.00144i | −0.00430i |
| (3,4) | 2.0 | 2.61 | 2.60865 | 2.60987 | 1.02676i | 0.10173i | 0.19710i |

method (RK4) for different initial conditions. The variation of the normalized amplitudes,

$$||A_j|| = \frac{|A_j|}{|A_j^0|}, \tag{34}$$

for $j = m, n, r$ with time for different initial conditions $A_j(t = 0) = A_j^0$ is illustrated in Fig. 5.

The rows from top to bottom in Fig. 5 correspond to $(m, n) = (1,3)$, $(1,4)$, $(2,3)$, $(2,4)$, and $(3,4)$, respectively, and the other parameters are given in Table III. For the initial conditions considered here, it can be seen from Fig. 5 that the absolute amplitudes of the two interacting primary waves (with amplitudes $A_m$ and $A_n$), having the same frequency $\omega$, increase or decrease simultaneously at a different rate. For the case of $(m, n) = (1, 4)$, $(2,3)$, $(2,4)$, and $(3,4)$, the amplitude of the secondary wave, $A_r$, increases or decreases when the amplitudes of the two interacting primary waves ($A_m$ and $A_n$) decrease or increase, respectively. In contrast, for $(m, n) = (1, 3)$, the amplitudes of all waves in a triad follow the same trend. It is also evident from Fig. 5 that the amplitudes of waves forming a triad depend on the mode numbers as well as the initial conditions. It is worth recalling that the waves of a resonant triad exchange energy continuously and, due to this, the amplitudes of the waves change in time.

### C. Equilibrium solution and linear stability

We shall now study the behavior of the equilibrium amplitude in the presence of a resonant triad. Let us write the amplitude equations (32) into real form, by assuming

$$A_m = |A_m|e^{i\theta_m(t)}, \quad A_n = |A_n|e^{i\theta_n(t)}, \quad A_r = |A_r|e^{i\theta_r(t)}, \quad \Theta = \theta_r - \theta_m - \theta_n. \tag{35}$$

Using (35), the six-dimensional system (32) reduces to a four-dimensional system,

$$\begin{aligned}
\frac{d|A_m|}{dt} &= \left(\lambda_m^{(r)}\cos\Theta - \lambda_m^{(i)}\sin\Theta\right)|A_n||A_r|,\\
\frac{d|A_n|}{dt} &= \left(\lambda_n^{(r)}\cos\Theta - \lambda_n^{(i)}\sin\Theta\right)|A_m||A_r|,\\
\frac{d|A_r|}{dt} &= \left(-\lambda_r^{(r)}\cos\Theta + \lambda_r^{(i)}\sin\Theta\right)|A_m||A_n|,\\
\frac{d\Theta}{dt} &= |A_m||A_n||A_r|\left[-\sin\Theta\left(\frac{\lambda_r^{(r)}}{|A_r|^2} + \frac{\lambda_n^{(r)}}{|A_n|^2} + \frac{\lambda_m^{(r)}}{|A_m|^2}\right) + \cos\Theta\left(\frac{\lambda_r^{(i)}}{|A_r|^2} - \frac{\lambda_n^{(i)}}{|A_n|^2} - \frac{\lambda_m^{(i)}}{|A_m|^2}\right)\right].
\end{aligned} \tag{36}$$

Since the coefficients $\lambda_m$, $\lambda_n$, and $\lambda_r$ are purely imaginary (see Table III), system (36) further reduces to

$$\begin{aligned}
\frac{d|A_m|}{dt} &= -\lambda_m^{(i)}|A_n||A_r|\sin\Theta, \quad \frac{d|A_n|}{dt} = -\lambda_n^{(i)}|A_m||A_r|\sin\Theta,\\
\frac{d|A_r|}{dt} &= \lambda_r^{(i)}|A_m||A_n|\sin\Theta, \quad \frac{d\Theta}{dt} = |A_m||A_n||A_r|\left(\frac{\lambda_r^{(i)}}{|A_r|^2} - \frac{\lambda_n^{(i)}}{|A_n|^2} - \frac{\lambda_m^{(i)}}{|A_m|^2}\right)\cos\Theta.
\end{aligned} \tag{37}$$

The equilibrium amplitudes are obtained by substituting $\frac{d|A_m|}{dt} = \frac{d|A_n|}{dt} = \frac{d|A_r|}{dt} = \frac{d\Theta}{dt} = 0$, which yields two types of equilibrium solutions:

(i) Pure-mode solutions in which the amplitudes of waves forming a resonant triad are independent,

$$\begin{aligned}
A_m| &= \mathcal{A}\sqrt{\mathrm{sgn}(\lambda_m^{(i)})A_1\,\lambda_m^{(i)}}, \quad |A_n| = \mathcal{A}\sqrt{\mathrm{sgn}(\lambda_n^{(i)})A_2\,\lambda_n^{(i)}}, \quad |A_r| = \mathcal{A}\sqrt{\mathrm{sgn}(\lambda_r^{(i)})A_3\,\lambda_r^{(i)}},\\
\Theta &= p\,\pi, \quad p = 0, \pm1, \pm2, \ldots,
\end{aligned} \tag{38}$$

where $\mathcal{A}$ is any nonzero positive constant and $A_i$, for $i \in 1, 2, 3$ are nonzero positive constants satisfying $\frac{\mathrm{sgn}(\lambda_n^{(i)})}{A_2} + \frac{\mathrm{sgn}(\lambda_m^{(i)})}{A_1} = \frac{\mathrm{sgn}(\lambda_r^{(i)})}{A_3}$. These solutions exist only when $\lambda_m^{(i)}$, $\lambda_n^{(i)}$, $\lambda_r^{(i)}$ are nonzero.

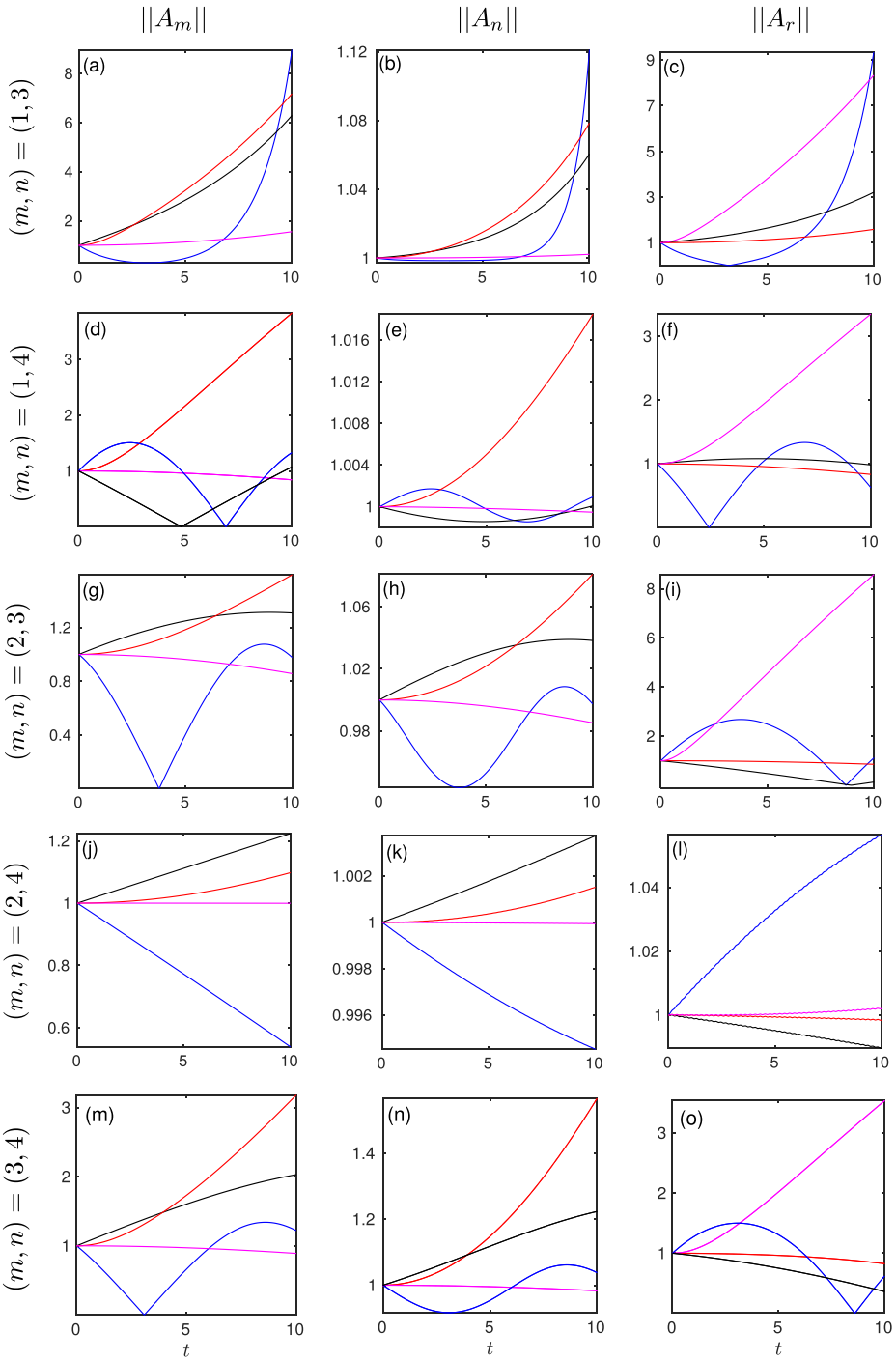


FIG. 5. Variation of the normalized amplitudes (34) with time for mode pairs $(m, n) = (1, 3), (1, 4), (2, 3), (2, 4), (3, 4)$ (depicted row-wise from top to bottom). The columns from left to right display $||A_m||$, $||A_n||$, and $||A_r||$, respectively. The initial conditions for $(A_m, A_n, A_r)$ are $(0.1 + 0.1i, 0.1 + 0.1i, 0.1)$ (black line); $(0.1, 0.1, 0.005)$ (magenta line); $(0.1i, 0.1i, 0.2)$ (red line), and $(0.6, 0.6, 0.2i)$ (blue line). Other parameters are the same as those listed in Table III.

Note that the governing equation for $\Theta$ [i.e., last equation of (37)] is invalid when at least one of $|A_m|$, $|A_n|$, and $|A_r|$ is zero. Thus, from the first three equations of (37), we get $\Theta = p\pi$, where $p$ is any integer.

(ii) Mixed-mode solutions in which the amplitude of the secondary wave in a triad is dependent on the amplitudes of the two primary waves,

$$A_m| = C_1, \quad |A_n| = C_2, \quad |A_r| = \frac{\sqrt{\lambda_r^{(i)}}|A_m||A_n|}{\sqrt{\lambda_m^{(i)}|A_n|^2 + \lambda_n^{(i)}|A_m|^2}}, \quad \Theta = p\pi, \quad p = 0, \pm 1, \pm 2, \ldots, \tag{39}$$

where $C_1$ and $C_2$ are positive constants. A mixed-mode solution (39) corresponds to a resonant triad.

In order to study the stability behavior of a resonant triad, we linearize (37) around the mixed-mode solution (39). Without loss of generality, we assume that $C_1 = C_2 = 1$, i.e., $|A_m| = |A_n| = 1$ and $|A_r| = \frac{\sqrt{\lambda_r^{(i)}}}{\sqrt{\lambda_m^{(i)}+\lambda_n^{(i)}}}$. The stability of the system (37) is determined by the eigenvalues of the Jacobian matrix,

$$\begin{bmatrix} 0 & 0 & 0 & \frac{\lambda_m^{(i)}\sqrt{\lambda_r^{(i)}}}{\sqrt{\lambda_m^{(i)}+\lambda_n^{(i)}}} \\ 0 & 0 & 0 & \frac{\lambda_n^{(i)}\sqrt{\lambda_r^{(i)}}}{\sqrt{\lambda_m^{(i)}+\lambda_n^{(i)}}} \\ 0 & 0 & 0 & -\lambda_r^{(i)} \\ -2\frac{\lambda_m^{(i)}\sqrt{\lambda_r^{(i)}}}{\sqrt{\lambda_m^{(i)}+\lambda_n^{(i)}}} & -2\frac{\lambda_n^{(i)}\sqrt{\lambda_r^{(i)}}}{\sqrt{\lambda_m^{(i)}+\lambda_n^{(i)}}} & -\left(\lambda_m^{(i)} + \lambda_n^{(i)}\right) & 0 \end{bmatrix}. \tag{40}$$

The four eigenvalues of the Jacobian matrix are

$$0, \quad 0, \quad \text{and} \quad \pm 2i\sqrt{\frac{\lambda_r^{(i)}\left(\lambda_m^{(i)2} + \lambda_m^{(i)}\lambda_n^{(i)} + \lambda_n^{(i)2}\right)}{\lambda_m^{(i)} + \lambda_n^{(i)}}}. \tag{41}$$

It is clear that the eigenvalues depend only on the coupled coefficients. Thus, the linear stability of system (37) can be ascertained by observing the signs of the imaginary part of coupled coefficients $\lambda_m^{(i)}$, $\lambda_n^{(i)}$, and $\lambda_r^{(i)}$. The following are two cases arising from RTIs among the different wave modes considered in this paper:

(i) The system is linearly stable if $\lambda_m^{(i)}$, $\lambda_n^{(i)}$, and $\lambda_r^{(i)}$ are of the same signs. From Table III, it is seen that for pairs $(m, n) = (2, 3)$ and (3,4), all the coefficients $\lambda_{m,n,r}^{(i)}$ are negative and positive, respectively. Thus, the linear stability analysis suggests that the system is stable when a triad involves primary waves with mode numbers as $(m, n) = (2, 3)$ and (3,4).

(ii) The system is linearly unstable if the sign of $\lambda_r^{(i)}$ is different from the other two. In this case, there exists an eigenvalue of (40) with positive real part. For $(m, n) = (1, 3)$, $(1, 4)$, and (2,4), the coefficients $\lambda_m^{(i)}$ and $\lambda_n^{(i)}$ are positive and $\lambda_r^{(i)}$ is negative; thus, a triad is unstable for all these cases (see Table III).

## V. SOLUTIONS UNDER THE PUMP-WAVE APPROXIMATION

Following Craik *et al.* [31], we solve (32) under the pump-wave approximation in which the amplitude, say $A_m$, of a primary wave in a resonant triad is much larger than the other two, say $A_n$ and $A_r$, i.e., $|A_m| \gg |A_n|, |A_r|$. Such a wave with the largest amplitude is referred to as the pump wave. Neglecting the effect of $A_n$ and $A_r$ on the evolution of $A_m$, the amplitude equations (32) reduce to

$$\frac{dA_m}{dt} = 0, \quad \frac{dA_n}{dt} = i\omega_n A_n + \lambda_n A_m^* A_r, \quad \frac{dA_r}{dt} = i\omega_r A_r + \lambda_r A_m A_n. \tag{42}$$

TABLE IV. Stability characteristics of the linearized system (43) when $A_m^0 = 100$. Other parameters are the same as in Table III.

| (m,n) | $\sigma_1$ | $\sigma_2$ | Stability characteristics |
|---|---|---|---|
| (1,3) | $2.004 + 6.765i$ | $-2.004 + 6.765i$ | Unstable |
| (1,4) | $4.447 + 6.315i$ | $-4.447 + 6.315i$ | Unstable |
| (2,3) | $-1.849i$ | $14.479i$ | Neutrally stable |
| (2,4) | $1.845i$ | $3.585i$ | Neutrally stable |
| (3,4) | $-10.305i$ | $18.135i$ | Neutrally stable |

The first equation gives $A_m(t) = A_m^0$, where $A_m^0$ is the initial amplitude of the pump wave. The other two equations of (42) form a linear system,

$$\frac{d}{dt}\begin{bmatrix} A_n \\ A_r \end{bmatrix} = \begin{bmatrix} i\omega_n & \lambda_n A_m^{0*} \\ \lambda_r A_m^0 & i\omega_r \end{bmatrix}\begin{bmatrix} A_n \\ A_r \end{bmatrix}. \tag{43}$$

The solution of (43) can be written in terms of the eigenvalues $\sigma_{1,2}$ and eigenvectors $\mathcal{V}_{1,2}$ of the matrix on the right-hand side of (43),

$$\begin{bmatrix} A_n \\ A_r \end{bmatrix} = b_1\, e^{\sigma_1 t}\boldsymbol{\mathcal{V}}_1 + b_2\, e^{\sigma_2 t}\boldsymbol{\mathcal{V}}_2, \tag{44}$$

where

$$\sigma_{1,2} = \pm\frac{1}{2}\sqrt{4\lambda_n\lambda_r\left|A_m^0\right|^2 - (\omega_n - \omega_r)^2} + i\frac{\omega_n + \omega_r}{2}, \tag{45}$$

$$\boldsymbol{\mathcal{V}}_{1,2} = \begin{bmatrix} \sqrt{4\lambda_n\lambda_r|A_m^0|^2 - (\omega_n - \omega_r)^2} \pm i(\omega_n - \omega_r) \\ \pm 2A_m^0\lambda_r \end{bmatrix}, \tag{46}$$

and $b_1$, $b_2$ are arbitrary constants that can be calculated from the predefined initial conditions on $A_n$ and $A_r$. Note that the eigenvalues depend on the amplitude of the pump wave $A_m^0$, which remains constant under the pump-wave approximation.

For illustration purposes, the initial amplitude of the pump wave is fixed to $A_m^0 = 100$. The amplitudes of other two waves, i.e., $A_n$ and $A_r$, are obtained numerically by solving (43). For each interaction case, the normalized amplitudes $||A_n||$ and $||A_r||$ [see (34)] of two smaller amplitude waves in the triad, i.e., mode $n$ and mode $r$, obtained from the numerical solution of (43) with the initial conditions $A_n^0 = A_r^0 = 0.01$ are illustrated in Fig. 6, where the other parameters are the same as given in Table III. In the case of $(m, n)$ equal to $(1, 3)$ and $(1, 4)$ [see Figs. 6(a)–6(d)], the normalized amplitudes increase monotonically with time and hence the amplitude functions become unbounded. For other mode pairs [see Figs. 6(e)–6(j)], the normalized amplitudes are periodic in nature, thereby the amplitude functions remain bounded. The above observation can also be seen in Fig. 7, which illustrates trajectories in the phase space associated with the dynamical system (42) from $t = 0$ to $t = 25$, with other parameters being the same as in Fig. 6. The amplitudes at the starting and ending times are marked by a (black) circle and a (red) square, respectively. It is seen from the figure that for all mode pairs except $(m, n) = (1, 3)$ and (1,4), the amplitudes $A_n$ and $A_r$ are oscillatory functions of time.

For the stability of a resonant triad when $A_m^0 = 100$, we determine the eigenvalues of the matrix on the right-hand side of (43) for different mode pairs $(m, n)$; see Table IV. As the entries of the matrix are complex, the eigenvalues may not appear as a complex conjugate pair. For the case of $(m, n) = (1, 3)$ and (1,4), there exists an eigenvalue with a positive real part (see the first and the second rows of Table IV), which implies that the amplitudes grow exponentially with time. On the

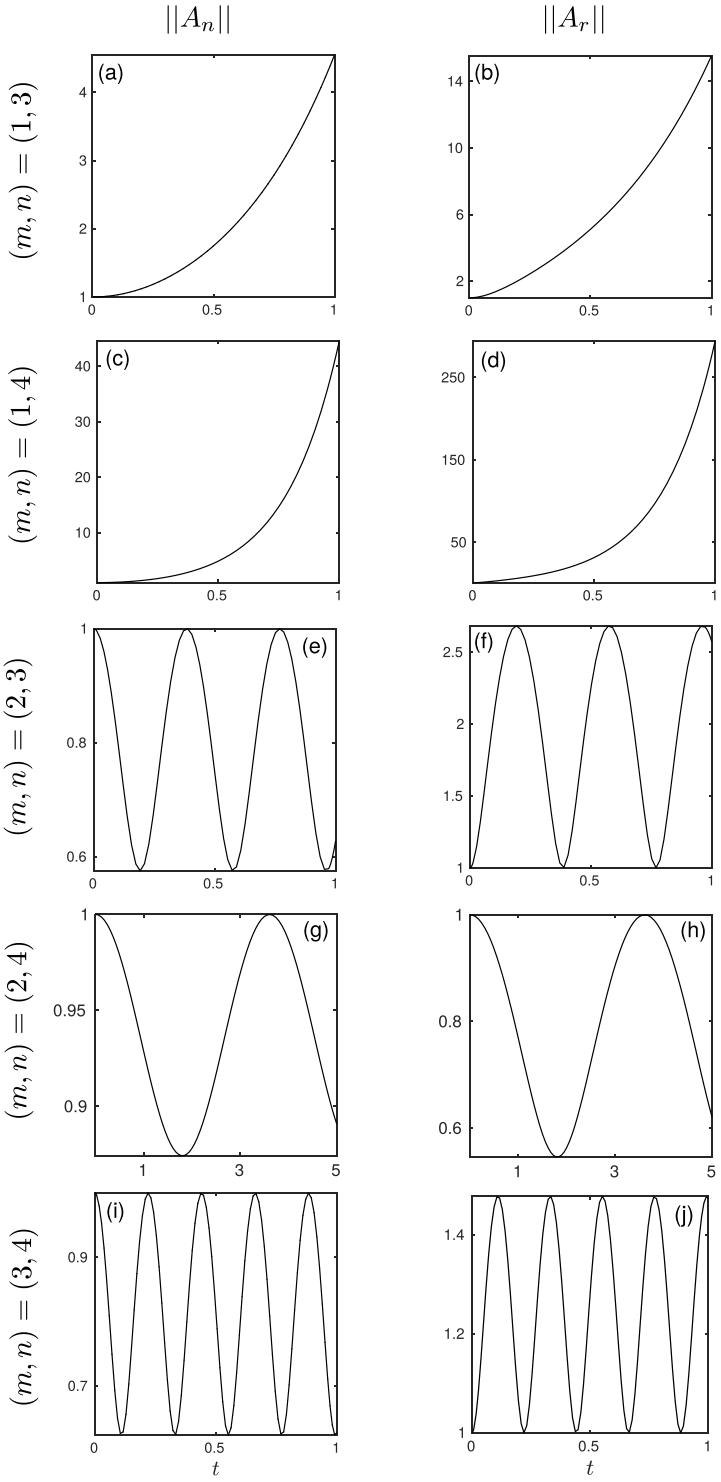


FIG. 6. Variation of the normalized amplitudes (34), $||A_n||$ (left column) and $||A_r||$ (right column), for various mode number pairs (top to bottom), obtained by solving (42) with $A_m^0 = 100, A_n^0 = A_r^0 = 0.01$. Other parameters used in each panel are listed in the respective rows of Table III.

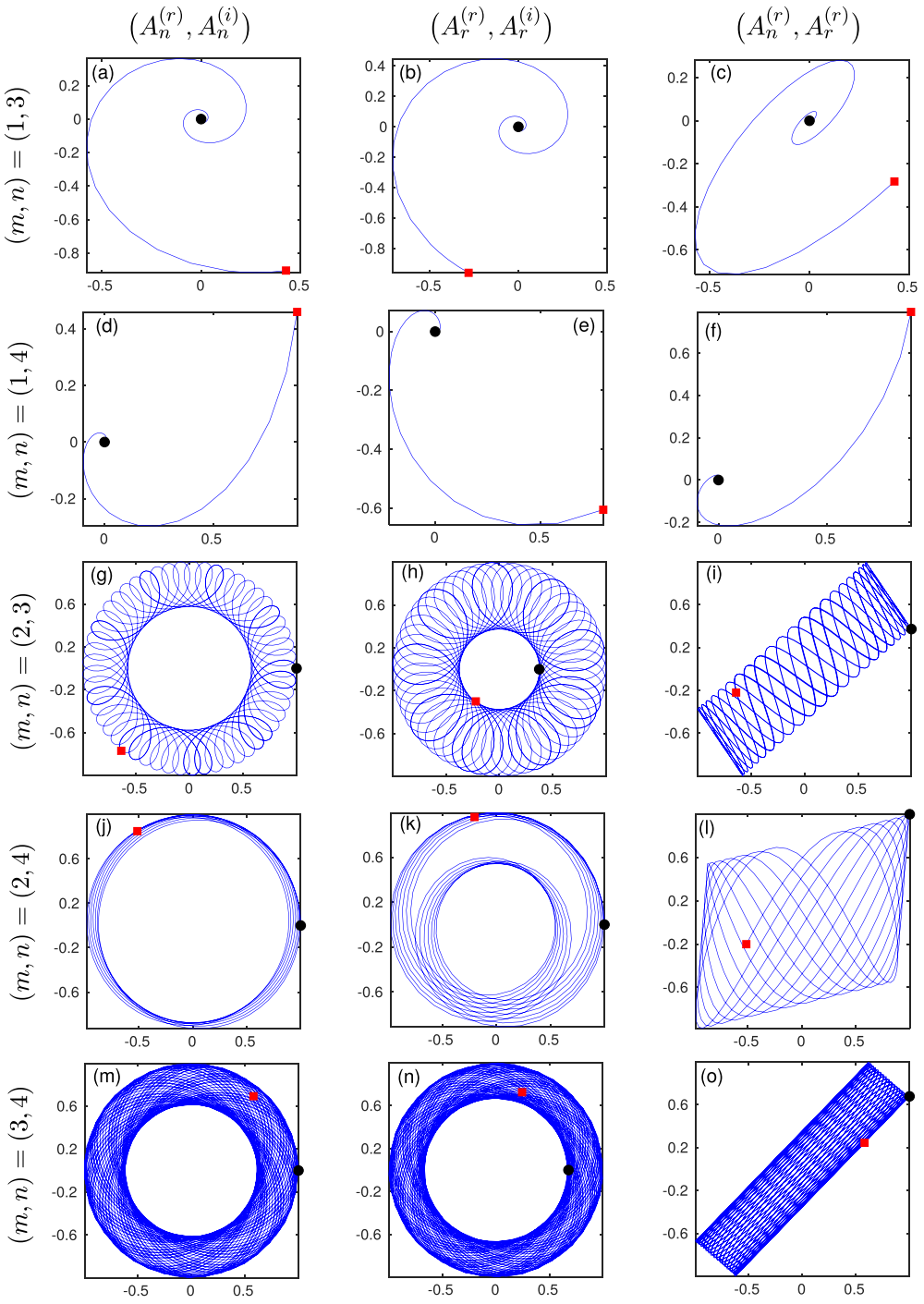


FIG. 7. Trajectories in the phase space for various mode number pairs (depicted row-wise) starting from dimensionless time $t = 0$ (marked by black circle) to $t = 25$ (marked by red square). The columns from left to right exhibit the trajectories in the $(A_n^{(r)}, A_n^{(i)})$, $(A_r^{(r)}, A_r^{(i)})$, and $(A_n^{(r)}, A_r^{(r)})$ planes, respectively. Here the amplitude of the pump wave is $A_m(t) = A_m^0 = 100$, and the initial amplitudes of the remaining waves in the triad are $A_n^0 = A_r^0 = 0.01$. Other parameters are listed in Table III.

other hand, for $(m, n) = (2, 3)$, (2,4), and (3,4), the real parts of both the eigenvalues are zero, and thus the amplitudes are periodic functions of time. The above conclusions are in tune with Figs. 6 and 7. It is clear that when the mode 1 primary wave acts as the pump wave, the amplitudes of other two waves present in the triad increase with time.

## VI. CONCLUSION

In the present paper, the stability of the resonant triad interactions (RTIs) of internal waves in an inviscid stably stratified uniform shear flow has been investigated. Specifically, we have focused on a situation wherein both the buoyancy frequency and the local Richardson number Ri are constant with $\mathrm{Ri} > 0.25$. As the system is considered to be vertically bounded between two parallel plates, the internal waves appearing in the system can be represented as the vertical modes satisfying the imposed boundary conditions on the top and bottom plates. The normal mode solution of the linear stability problem has been expressed in terms of the modified Bessel functions of complex order, which represent the vertical structures of internal wave modes. From linear stability analysis, it has been found that the frequency of each forward mode increases with increasing Ri, and the frequency of the first mode increases the most rapidly.

In contrast to the no-shear case, resonant triads comprised of the primary modes $(1, 3)$ and $(1, 4)$ and the corresponding superharmonic modes do exist in the present system. In a nutshell, the presence of the uniform shear can render RTIs, which otherwise are not possible in the absence of shear. It has also been verified that due to uniform shear in the flow, the exact mode number of the secondary mode cannot be determined in terms of the mode numbers of the primary modes. Thus, the mode number of the secondary mode in a triad has been extracted in two ways: (i) by observing the vertical structure of the secondary wave and (ii) by analyzing the wave numbers associated with the mode at frequency $2\omega$, as shown in Table II.

The frequency $\omega$, which gives rise to a resonant triad, has been identified for various mode-number pairs. The amplitude equations of a resonant triad comprised of two primary internal modes, with mode numbers $m$ and $n$, having the same frequency $\omega$, and a secondary (superharmonic) mode, with mode number $r$, of frequency $2\omega$ have been derived through the orthogonality conditions. The coupling coefficients, linked with the nonlinear terms in the amplitude equations, have been computed numerically for the interaction among two primary internal modes of mode numbers $m$ and $n$, with $m, n \in \{1, 2, 3, 4\}$, and a superharmonic mode of mode number $r$. For various interaction cases, these coefficients have been calculated and are presented in Table III. It turns out that all coupling coefficients are purely imaginary numbers in the present case of the uniformly stratified uniform shear flow.

The amplitude equations have been solved numerically using the RK4 method. It has been shown that the evolution of the amplitudes of the waves involved in RTIs depends on the mode numbers as well as on the initial conditions. In other words, the amplitude of the superharmonic wave may increase or decrease depending on the mode numbers and initial conditions, irrespective of the amplitudes of the primary interacting waves present in a triad. For the chosen parameters, the linear stability around the mixed-mode equilibrium solution shows that resonant triads are stable when the primary waves with the mode-number pairs (2,3) and (3,4) interact. In contrast, resonant triads are unstable for interactions among the primary waves with mode-number pairs as (1,3), (1,4), and (2,4). The results discussed in this paper provide a qualitative analysis of the stability of the waves forming RTIs.

The solutions under the pump-wave approximation have also been illustrated in detail, wherein the primary wave having the lowest mode number is considered as the pump wave. The cases of RTIs leading to oscillatory bounded and unbounded solutions have been analyzed. In the considered configuration, the bounded solutions for the tested Ri values have been found to be periodic in nature and to be related to interactions among the second-fastest primary mode (mode 2) onward. In contrast, the interactions involving the fastest primary mode (mode 1) have been found to be unstable. Under the pump-wave approximation, the phase-space trajectories of the dynamical

system, formed by the differential equations governing the amplitudes of the waves forming a triad, have been portrayed. Interestingly, for the chosen parameters, it has been found that the presence of a high-amplitude primary wave having mode number $\geqslant 2$ in a resonant triad makes the system stable. To summarize, the stability of resonant triads depends on the system parameters (for instance, frequency, mode numbers, local Richardson number) as well as on the initial amplitudes of the interacting waves.

The results presented in this paper are the first step to understand energy transfer among different wave modes present in a resonant triad. Although the derivation and analysis performed here are for an inviscid stratified uniform shear flow, the work can readily be extended to more realistic scenarios, for instance, oceanlike stratifications, where the stratification can be nonuniform. Furthermore, the present analysis is also expected to pave the way to handle more general wave interactions arising in many fluid-wave interaction problems with or without resonance. To predict the existence and stability of RTIs in a more realistic scenario, one must include the effect of three dimensionality, nonuniform stratifications, Earth's rotation, viscosity, and diffusivity in the present idealized problem. The inclusion of all these effects may significantly affect the formation of RTIs and their stability, which will be an interesting topic of future research.

## ACKNOWLEDGMENTS

The authors gratefully acknowledge the anonymous reviewers and the editor Professor Bruce Sutherland for their valuable suggestions, which significantly improved the article. The authors also thank Manuel Torrilhon, Dr. Vinay Kumar Gupta, and Dr. Anubhab Roy for fruitful discussions. L.B. gratefully acknowledges NBHM (India) for financial support and P.S. gratefully acknowledges financial support from IIT Madras through Grant No. MAT/16-17/671/NFSC/PRIY.

[1] O. S. Lee, Observation on internal waves in shallow water, Limnol. Oceanogr. **6**, 312 (1961).
[2] B. A. Hughes and H. L. Grant, The effect of internal waves on surface wind waves 1. Experimental measurements, J. Geophys. Res. **83**, 443 (1978).
[3] B. A. Hughes, The effect of internal waves on surface wind waves 2. Theoretical analysis, J. Geophys. Res. **83**, 455 (1978).
[4] R. Grimshaw, E. Pelinovsky, T. Talipova, and A. Kurkin, Simulation of the transformation of internal solitary waves on oceanic shelves, J. Phys. Oceanogr. **34**, 2774 (2004).
[5] J. S. Turner, *Buoyancy Effects in Fluids* (Cambridge University Press, Cambridge, 1973).
[6] C. Garrett and W. Munk, Internal waves in the ocean, Annu. Rev. Fluid Mech. **11**, 339 (1979).
[7] C. Staquet and J. Sommeria, Internal gravity waves: From instabilities to turbulence, Annu. Rev. Fluid Mech. **34**, 559 (2002).
[8] B. R. Sutherland, *Internal Gravity Waves* (Cambridge University Press, Cambridge, 2010).
[9] C. Garrett, Internal tides and ocean mixing, Science **301**, 1858 (2003).
[10] L. St. Laurent and C. Garrett, The role of internal tides in mixing the deep ocean, J. Phys. Oceanogr. **32**, 2882 (2002).
[11] C. Wunsch and R. Ferrari, Vertical mixing, energy, and the general circulation of the oceans, Annu. Rev. Fluid Mech. **36**, 281 (2004).
[12] G. I. Taylor, Effect of variation in density on the stability of superposed streams of fluid, Proc. R. Soc. London A **132**, 499 (1931).
[13] S. Goldstein, On the stability of superposed streams of fluids of different densities, Proc. R. Soc. London A **132**, 524 (1931).
[14] K. M. Case, Stability of an idealized atmosphere. I. Discussion of results, Phys. Fluids **3**, 149 (1960).
[15] F. J. Dyson, Stability of an idealized atmosphere. II. Zeros of the confluent hypergeometric function, Phys. Fluids **3**, 155 (1960).

[16] A. Davey and W. H. Reid, On the stability of stratified viscous plane Couette flow. Part 1. Constant buoyancy frequency, J. Fluid Mech. **80**, 509 (1977).
[17] A. D. D. Craik, *Wave Interactions and Fluid Flows*, Cambridge Monographs on Mechanics (Cambridge University Press, Cambridge, 1986).
[18] O. M. Phillips, Wave interactions - The evolution of an idea, J. Fluid Mech. **106**, 215 (1981).
[19] O. M. Phillips, On the dynamics of unsteady gravity waves of finite amplitude Part 1. The elementary interactions, J. Fluid Mech. **9**, 193 (1960).
[20] M. S. Longuet-Higgins, Resonant interactions between two trains of gravity waves, J. Fluid Mech. **12**, 321 (1962).
[21] K. Hasselmann, On the non-linear energy transfer in a gravity-wave spectrum Part 1. General theory, J. Fluid Mech. **12**, 481 (1962).
[22] R. M. Moreira and D. H. Peregrine, Nonlinear interactions between deep-water waves and currents, J. Fluid Mech. **691**, 1 (2012).
[23] S. B. Yoon and P. L.-F. Liu, Interactions of currents and weakly nonlinear water waves in shallow water, J. Fluid Mech. **205**, 397 (1989).
[24] K. M. Watson and B. J. West, A transport-equation description of nonlinear ocean surface wave interactions, J. Fluid Mech. **70**, 815 (1975).
[25] P. Ripa, On the theory of nonlinear wave-wave interactions among geophysical waves, J. Fluid Mech. **103**, 87 (1981).
[26] J. Vanneste, Explosive resonant interaction of baroclinic Rossby waves and stability of multilayer quasi-geostrophic flow, J. Fluid Mech. **291**, 83 (1995).
[27] J. W. Miles, Obliquely interacting solitary waves, J. Fluid Mech. **79**, 157 (1977).
[28] T. Dauxois, S. Joubaud, P. Odier, and A. Venaille, Instabilities of internal gravity wave beams, Annu. Rev. Fluid Mech. **50**, 131 (2018).
[29] B. R. Sutherland and R. Jefferson, Triad resonant instability of horizontally periodic internal modes, Phys. Rev. Fluids **5**, 034801 (2020).
[30] A. D. D. Craik, and K. Stewartson, Evolution in space and time of resonant wave triads II. A class of exact solutions, Proc. R. Soc. London A **363**, 257 (1978).
[31] A. D. D. Craik, J. A. Adam, and K. Stewartson, Evolution in space and time of resonant wave triads I. The 'pump-wave approximation', Proc. R. Soc. London A **363**, 243 (1978).
[32] L. Engevik, An amplitude-evolution equation for linearly unstable modes in stratified shear flows, J. Fluid Mech. **117**, 457 (1982).
[33] A. D. D. Craik, Resonant gravity-wave interactions in a shear flow, J. Fluid Mech. **34**, 531 (1968).
[34] R. Grimshaw, Resonant wave interactions in a stratified shear flow, J. Fluid Mech. **190**, 357 (1988).
[35] K. Hasselmann, A criterion for nonlinear wave stability, J. Fluid Mech. **30**, 737 (1967).
[36] M. Tsutahara, Resonant interaction of internal waves in a stratified shear flow, Phys. Fluids **27**, 1942 (1984).
[37] J. M. Becker and R. H. J. Grimshaw, Explosive resonant triads in a continuously stratified shear flow, J. Fluid Mech. **257**, 219 (1993).
[38] S. A. Thorpe, On wave interactions in a stratified fluid, J. Fluid Mech. **24**, 737 (1966).
[39] C. Canuto, M. Hussaini, A. M. Quarteroni, and T. A. Zang, *Spectral Methods in Fluid Dynamics 6* (Springer-Verlag, Berlin, 1988).
[40] A. Eliassen, E. Høiland, and E. Riis, *Two-dimensional Perturbation of a Flow with Constant Shear of a Stratified Fluid* (Institute of Theoretical Astrophysics, Institute for Weather, Climate Research, Oslo, 1953).
[41] L. Engevik, A note on a stability problem in hydrodynamics, Acta Mech. **12**, 143 (1971).
[42] G. N. Watson, *A Treatise on the Theory of Bessel Functions* (Cambridge University Press, Cambridge, 1995).
[43] P. J. Schmid and D. S. Henningson, *Stability and Transition in Shear Flows* (Springer, New York, 2001).